http://dx.doi.org/10.5012/bkcs.2013.34.8.2271

Reduced Titania Films with Ordered Nanopores and Their Application to Visible Light Water Splitting

Muhammad Shahid, Seo-Yeong Choi, Jingling Liu, and Young-Uk Kwon*

*Department of Chemistry, BK-21 School of Chemical Materials Science, SKKU Advanced Institute of Nanotechnology, Sungkyunkwan University, Suwon 440-746 Korea. *E-mail: ywkwon@skku.edu*
Received March 28, 2013, Accepted May 3, 2013

We report on the photoelectrochemical properties of partially reduced mesoporous titania thin films. The fabrication is achieved by synthesizing mesoporous titania thin films through the self-assembly of a titania precursor and a block copolymer, followed by aging and calcination, and heat-treatment under a H_2 (1 torr) environment. Depending on the temperature used for the reaction with H_2, the degree of the reduction (generation of oxygen vacancies) of the titania is controlled. The oxygen vacancies induce visible light absorption, and decrease of resistance while the mesoporosity is practically unaltered. The photoelectrochemical activity data on these films, by measuring their photocurrent-potential behavior in 1 M NaOH electrolyte under AM 1.5G 100 mW cm^{-2} illumination, show that the three effects of the oxygen vacancies contribute to the enhancement of the photoelectrochemical properties of the mesoporous titania thin films. The results show that these oxygen deficient TiO_2 mesoporous thin films hold great promise for a solar hydrogen generation. Suggestions for the materials design for improved photoelectrochemical properties are made.

Key Words : Mesoporous titania thin film, Oxygen vacancy, Photoelectrochemical (PEC) property

Introduction

Since the first report on the photochemical splitting of water on a TiO_2 electrode by Fujishima and Honda,[1] water splitting by using semiconductors has attracted tremendous interests for the generation of clean and renewable hydrogen fuel directly from solar irradiation. Among different morphologies of TiO_2, those with 3D mesopores have attracted strong interests because they have large surface areas and the pores can allow fast access of reactive gases and liquids.[2-5]

Mesoporous films of TiO_2 formed by dispersing nanoparticles have been studied for photocatalytic hydrogen evolution.[6] Recently, it has been demonstrated that mesoporous TiO_2 films via the self-assembly process outperform those through the assembly of pre-formed TiO_2 nanoparticles.[7] The authors argue that the inter-particle boundaries in the latter give rise to high resistance for photo-generated electrons or holes.

On the other hand, TiO_2 in the stoichiometric state has the problems of the inability to utilize visible light. To overcome this limitation, many authors have explored different approaches ranging from doping with metals[8] or non-metals[9-11] to loading with noble metals.[12,13] The dopants introduce impurity states in various positions in the band gap of TiO_2 and lead to different degrees of modification in the electronic structure.[14] Oxygen vacancies are known to form shallow donor states in TiO_2, with relatively low formation energies.[15] It has been reported that oxygen vacancies play a critical role in determining the surface and electronic properties of TiO_2.[16]

The heat treatment in H_2 atmosphere is a usual method to produce oxygen vacancies of TiO_2 for the improvement of photoelectrochemical (PEC) performance and photocatalytic efficiency.[17,18] Many investigators have studied the effects of heat-treatment conditions such as temperatures, time, H_2-pressure.[19,20] However, we note that there has been no report on the effect of H_2 treatment of mesoporous TiO_2 in relation with PEC or photocatalysis.

In this study, we have combined the above mentioned two desirable features to be incorporated in the TiO_2 electrodes for PEC applications. That is, we synthesized mesoporous films of reduced titania. Previously, we synthesized mesoporous titania thin films (MTFs) with highly well-ordered pores.[21] In the present study, we heat-treated MTFs to produce reduced mesoporous titania films (R-MTFs), and characterized them as PEC electrodes. The R-MTFs have large surface areas and short diffusion distances for the electrolyte, which is expected to facilitate the charge separation and, thus, reduce the loss due to electron hole recombination, resulting in the enhancement of PEC performance.

Experimental

R-MTFs were obtained by reducing MTFs with H_2 at elevated temperatures. MTFs was formed by spin coating a precursor solution on FTO (Fluorine-doped tin oxide, Arrandee) electrodes, followed by aging and calcination. The details of the synthesis and characterization are described in our previous paper.[21] Briefly, the precursor solution prepared by mixing 0.5 g of a Pluronic triblock copolymer surfactant F127 ($EO_{106}PO_{70}EO_{106}$; EO = ethylene oxide, PO = propylene oxide) in 10 g of absolute ethanol (Samchun, 99.9%) with 1.1 mL of $TiCl_4$ (Aldrich) was spun-cast on FTO (1 × 1 cm^2) substrates, aged under 18 °C and relative

humidity of 80% condition, and calcined at 300 °C in the air. The MTFs were further heat-treated under a reductive condition of 1 torr hydrogen for 10 hrs to obtain R-MTFs. The temperature was controlled to be 350, 400, or 450 °C with a heating/cooling rate of 1 °C/min.

The pore structures of the MTFs were characterized by low-angle X-ray diffraction (XRD; Rigaku D/Max-2200, Cu Kα (λ = 1.5415 Å)), field emission scanning electron microscopy (FESEM; JSM-7000F), transmission electron microscopy (TEM; JEOL JEM-3010). For TEM observation, tiny slices of samples scrapped from the films were dispersed in ethanol and the resultant solution was dropped on a carbon-coated Cu grids. The UV-Vis absorbance (UV-Vis) of the as-prepared samples was measured with a UV-Vis spectrometer (Shimadzu UV-2500). Photocurrent-potential responses (I-V curves) were recorded with a 150 W Xenon lamp-based solar simulator (PECCELL, Yokohama, Japan, PECL01: 100 mW cm^{-2}). The light intensity was calibrated using a silicon reference cell (Fraunhofer ISE, Certificate No. CISE269). An aqueous 1 M NaOH solution was employed as an electrolyte. The PEC characteristics of these electrodes in a 1 M NaOH(aq) solution were measured by using a three electrode cell with a Ag/AgCl/sat'd KCl as the reference electrode and a Pt-gauge as the counter electrode under AM 1.5G illumination (100 mW cm^{-2}).

Results and Discussion

The MTFs used in the present study are characterized by the 3D pore network derived from the Im-3m self-assembly structure of the spin-cast films. The Im-3m structure is also called as the cage-like structure because there are large spherical pores at the center and the corner of the cubic unit cell. The large pores connect to the next ones along the [111] directions to form a 3D pore network. In our synthesis method, the Im-3m structure is preferentially oriented to have the [111] direction perpendicular to the surface. Therefore, upon removal of the template F127 and consolidation of the titania wall during the calcination, the films undergo uniaxial shrinkage in the surface normal direction, inducing the fusion of adjacent cages along the [111] direction into vertical channels. The resultant films show hexagonally ordered pores when viewed from the top (Figure 1(a)). Depending on the degree of the shrinkage, these vertical channels are also connected to neighboring ones.[21,22]

The MTFs synthesized by calcination at 300 °C were further heat-treated under an H_2 atmosphere (1 torr) at different temperatures to produce R-MTFs. The R-MTF samples will be denoted with the heating temperature as in R-MTF-400 for the sample obtained by heating at 400 °C.

The SEM images in Figure 1 show that the initial pore morphology of MTF is maintained in R-MTFs. The TEM images in the insets also support this observation. However, one can also see that the pores are slightly deformed as the temperature is 400 °C or higher. The small angle XRD patterns in Figure 2 show a peak that can be attributed to the (111) mesoscopic ordering. The other peaks are absent

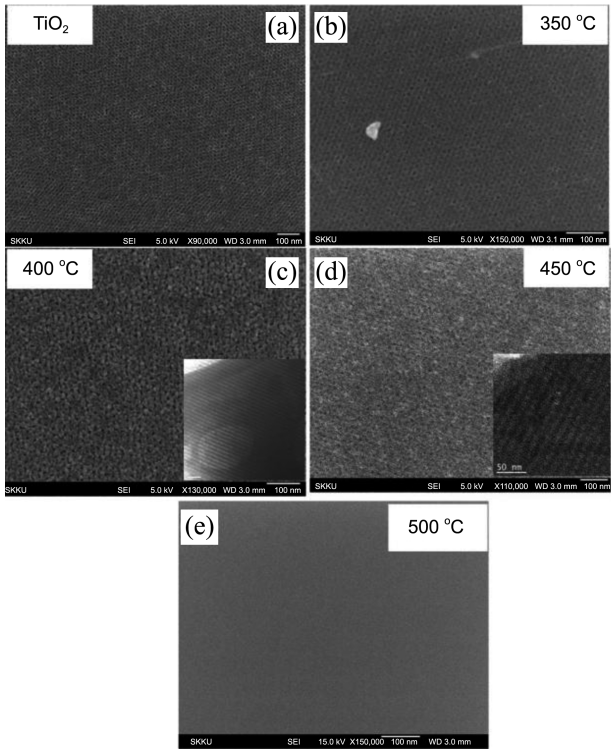

Figure 1. SEM images of MTF and R-MTFs. (a) MTF, (b) R-MTF-350, (c) R-MTF-400, (d) R-MTF-450, and (e) R-MTF-500. Insets in (c) and (d) are TEM images.

because of the preferential orientation of MTF. This peak remains unchanged in R-MTF-350. However, its position is shifted to higher angles in R-MTF-400 and R-MTF-450, indicating the decrease of the interplane distance, which agrees with the above-mentioned film shrinkage.[23,24] The decrease of the peak intensity in these samples is ascribed to the fusion of the cage-like pores into vertical channels decreasing the contrast of the electron density. We also tried 500 °C in the hydrogen treatment of MTF. However, at this temperature, the mesoporosity is completely lost as shown in Figure 1(e). For this reason, R-MTF-500 was not studied

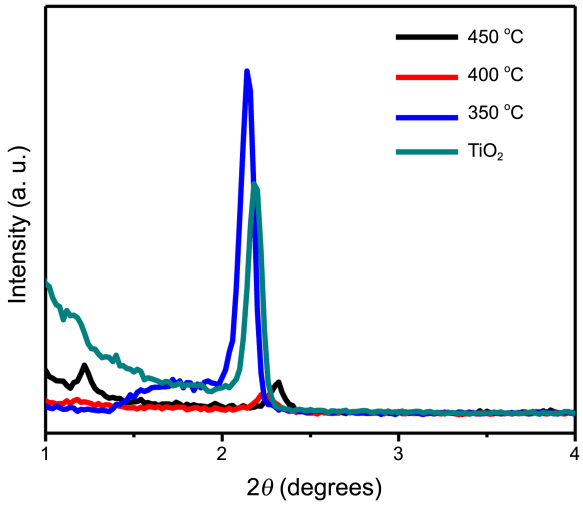

Figure 2. Small-angle XRD patterns of MTF and R-MTFs.

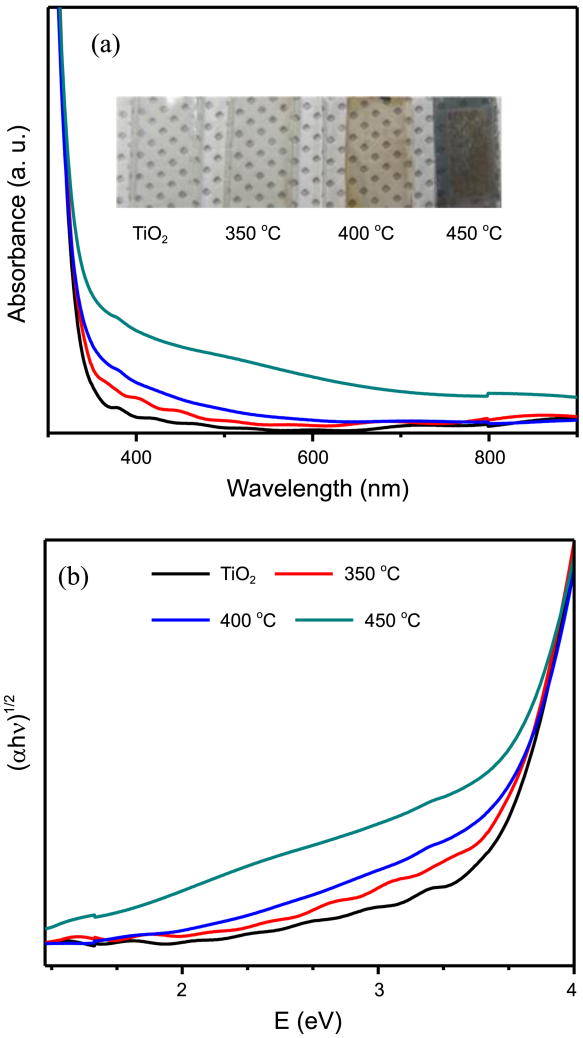

Figure 3. (a) UV-Vis spectra and (b) the Tauc plots of $(\alpha h\nu)^{1/2}$ *vs.* hn of MTF and R-MTFs. Inset in (a) are the pictures of MTF and R-MTFs.

any further.

The optical properties of R-MTFs are also affected by the temperature of hydrogen treatment. The original MTF is transparent to the visible light. R-MTF-350 has almost the same appearance as MTF although its UV-Vis spectrum shows an increased absorption of short wavelength visible photons ($\lambda < 400$ nm). By contrast, R-MTF-400 is light brown and R-MTF-450 is grayish. The UV-Vis absorption spectra of these samples in Figure 3(a) account for the corresponding colors. From the Tauc plot of the absorption spectrum of MTF in Figure 3(b), its band gap energy is calculated to be 3.3 eV, slightly larger than that of anatase (3.2 eV),[25,26] probably because of the thin titania walls of MTF, ~4 nm. The Tauc plots of R-MTFs show that the original band gap of TiO_2 is practically unaffected by the reduction. Instead, there are many mid-gap levels created with the density increasing with the temperature of the reduction reaction. With spectroscopic data, it is clear that R-MTFs can utilize visible photons in PEC.

In order to assess the potential of R-MTFs for PEC application, we investigated their photocurrent responses. It is well known that photocurrent response is an indirect way to measure the rate of production of hydrogen and oxygen through splitting of water. It reflects the number of charge carriers produced from the incident light and their subsequent participation in water oxidation on the photoanode

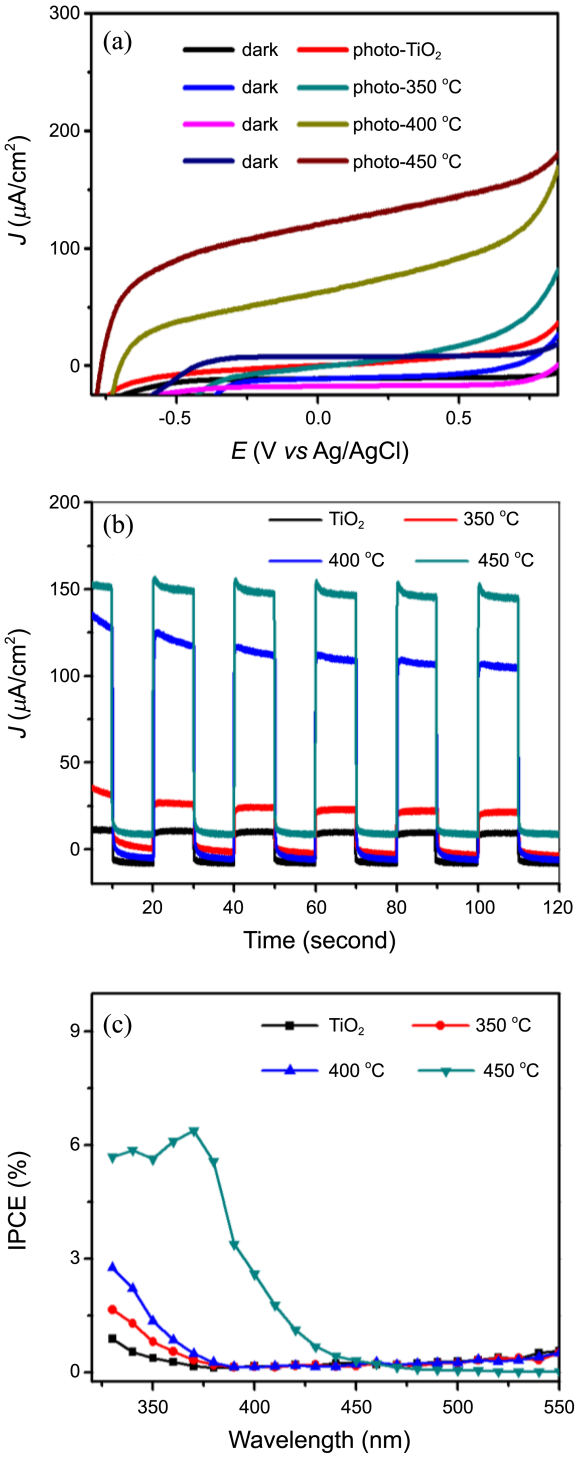

Figure 4. (a) I-V curves of MTF and R-MTFs in 1 M NaOH under 100 mW·cm^{-2} illumination. (b) Chopped photocurrent of MTF and R-MTFs at a potential of +0.6 V *vs.* Ag/AgCl. (c) IPCE spectra of MTF and R-MTFs at a potential of +0.6 V *vs* Ag/AgCl.

and the hydrogen ion reduction on the counter electrode.[27,28] As shown in the plots of current density as a function of applied potential in Figure 4(a), MTF and R-MTF-350 show insignificant photocurrent effects, which can be explained with their low level of absorption of visible photons. By contrast, R-MTF-400 and R-MTF-450 show significantly increased photocurrent responses. The photocurrent of R-MTF-450 is higher than that of R-MTF-400. Clearly, the partial reduction of TiO_2 by H_2 treatment makes a positive effect.

It is well-known that H_2-treatment of early transition metal oxides induces the formation of oxygen defects and the reduction of the transition metal. In the present case, some of the Ti^{4+} ions are reduced to Ti^{3+}, which effectively creates doner level.[29,30] As a result, the conduction electron density is increased, the resistance is decreased, and the Fermi level is raised, all of which will be beneficial features of reduced titania in PEC in addition to the increase of visible light absorption shown in Figure 3. These effects will become stronger as the amount of reduction increased, which can be controlled by the temperature of the H_2-treatment. Unfortunately, the temperature is limited to be below 500 °C for the present MTF because the porous structure is disrupted at 500 °C.

Our data show evidences, directly or indirectly, for the changes in the electronic structure of titania upon reduction. In Figure 4(b), the dark currents of R-MTF samples are increased from that of MTF, which may be attributed to the decrease of the internal resistance of R-MTFs materials.[31] The onset potentials of the photocurrents of R-MTF-400 and R-MTF-450 are measured to be −0.7 and −0.77 V (*vs.* Ag/AgCl), respectively, which may reflect the different Fermi levels of these materials. In Figure 5, we show the variation of photoconversion efficiencies of MTF and R-MTFs as a function of the applied bias potential. The efficiency is calculated by using the equation:

$$\eta\,(\%) = j_p \times (1.23 - V_b)/P$$

where, j_p is the photocurrent density (mA cm^{-2}), P is the incident light intensity (mW cm^{-2}), and V_b is the bias voltage which is applied in the two electrodes system.[28]

Two major observations of this plot are: First, MTF and R-MTF-350 have photoconversion efficiencies smaller than zero at all bias potential range. This means that the photocurrents of these electrodes, if any, are mainly driven by the applied bias potential, not by the internal field between the electrodes. On the contrary, R-MTF-400 and R-MTF-450 show positive efficiencies as seen before. The photoconversion efficiency of MTF-450 was calculated to be 0.09% at −0.46V *vs* Ag/AgCl. Second, the efficiency maximum is negatively shifted as the degree of reduction increases. This behavior agrees with the rise of the Fermi level by reduction. In case of R-MTF-450, although the photocurrent is measured with a bias potential of +0.6 V in Figure 4(b), photocurrent can be observed even under zero bias.

We note that the efficiency of R-MTF-350 is even lower than that of MTF. At present, the reason is not clear. Probably, when the doping level is too low, the doping states function as the trap sites instead of inducing above mentioned positive effects of doping.

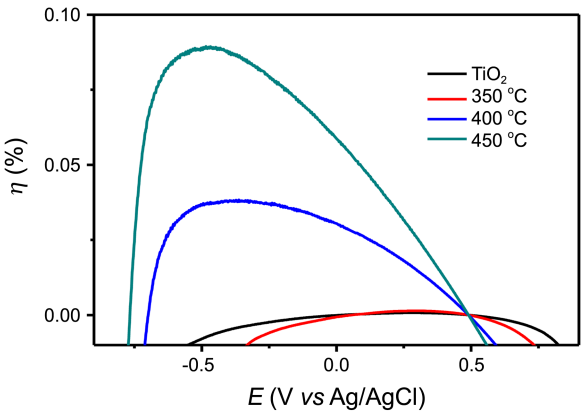

Figure 5. Variation of PEC efficiency of MTF and R-MTF with the applied potential.

The incident photon-to-current conversion efficiencies (IPCE) of MTF and R-MTFs as a function of the wavelength of monochromatic irradiation were studied at a constant bias (+0.6 V *vs* Ag/AgCl) in a 1 M NaOH(aq) solution (Figure 4(c)).[32] The IPCE increases with the increase of the degree of reduction in R-MTF. MTF, R-MTF-350 and -400 show maximum IPCE values wavelengths shorter than 350 nm. By contrast, the IPCE maximum of R-MTF-450 is red-shifted to 375 nm. Furthermore, the peak current is drastically increased from ~1% for MTF to ~6% for R-MTF-450.

Our results demonstrate that synthesizing mesoporous titania thin films and reducing them can be a viable strategy to fabricate efficient PEC electrodes. However, at the same time, the efficiency of our R-MTF is not high enough for practical applications. We consider that there are a number of ways to improve the efficiency. (1) The film thickness has to be optimized to absorb the optimum amount of photons. In the present study, the film thickness of MTF is ~200 nm (data not shown).[21] By controlling the spinning rate during the spin-coating of the precursor solution, the film thickness can be controlled to ~500 nm. If necessary, the spin-coating can be repeated to increase the film thickness to a few μm. (2) The degree of reduction also can be controlled. Generally, the mesoporous structure of MTF can withstand up to 450 °C, which sets the limit of the degree of reduction of R-MTFs. However, we believe that if higher pressure of H_2 is used, it may be possible to achieve higher levels of reduction without increasing the temperature too high. (3) In order to use the most of the mesoporosity of MTFs, the pore size has to be tuned to allow the easy flow of electrolyte. The pore size can be controlled by using different kinds of block copolymers in the formation of the self-assembly structures. At present, F127 is the largest block copolymer adaptable to our synthesis procedure, limiting the largest pores size to be about 7 nm. However, there have been reports on using home-made block copolymers to produce mesoporous thin films with larger pores.[33,34] (4) Finally, the wall thickness of

the MTFs must be controlled. The present MTF is composed of 4 nm thick titania walls. This certainly cannot be the optimal thickness. The larger band gap of MTF (3.3 eV) than the bulk value (3.0 eV or 3.2 eV) indicates this is so. Fortunately, there have been a few methods to increase the wall thickness reported in the literature.[35,36] With some or all of these measures employed, it seems possible to develop highly efficient PEC electrodes based on reduced mesoporous titania film films.

Conclusion

In the present work, we successfully fabricated reduced well ordered mesoporous titania thin films (R-MTFs), which show promising properties for water splitting. The films are characterized by regularly ordered 3D pores and high levels of oxygen vacancies on the titania wall. The oxygen vacancies are introduced through the reaction with hydrogen at elevated temperatures. With the hydrogen pressured fixed at 1 torr, the reaction temperature determines the degree of the reduction. As the degree of reduction increases, the absorption of the visible light increases, the conductivity increases, and the surface activity increases. There are many different ways the photoelectrochemical properties of the present mesoporous titania thin films can be improved. The capability of making highly photoactive mesoporous titania film opens up new opportunities in various areas, including PEC water splitting, dye-sensitized solar cells, and photocatalysis. Investigations of such possibilities are under progress in our group.

Acknowledgments. This work was supported by grants NRF-20090081018 (Basic Science Research Program), NRF-2011-0031392 (Priority Research Center Program), NRF-2009-0083540 (Basic Science Research Program), and R31-10029 (World Class University Program). We thank CCRF for the TEM. We thank Prof. J. H. Park for the PEC data.

References

1. Fujishima, A.; Honda, K. *Nature* **1972**, *238*, 37.
2. Juan, L. V.-E.; Ya-Dong, C.; Kevin, C. W. W.; Yusuke, Y. *Sci. Technol. Adv. Mater.* **2012**, *13*, 013003.
3. Carreon, M. A.; Choi, S. Y.; Mamak, M.; Chopra, N.; Ozin, G. A. *Journal of Materials Chemistry* **2007**, *17*, 82.
4. Hou, K.; Tian, B.; Li, F.; Bian, Z.; Zhao, D.; Huang, C. *Journal of Materials Chemistry* **2005**, *15*, 2414.
5. Hung, I. M.; Wang, Y.; Lin, L.-T.; Huang, C.-F. *J. Porous Mater* **2010**, *17*, 509.
6. Korzhak, A. V.; Ermokhina, N. I.; Stroyuk, A. L.; Bukhtiyarov, V. K.; Raevskaya, A. E.; Litvin, V. I.; Kuchmiy, S. Y.; Ilyin, V. G.; Manorik, P. A. *Journal of Photochemistry and Photobiology A: Chemistry* **2008**, *198*, 126.
7. Hartmann, P.; Lee, D.-K.; Smarsly, B. M.; Janek, J. *ACS Nano* **2010**, *4*, 3147.
8. Bae, S. W.; Borse, P. H.; Hong, S. J.; Jang, J. S.; Lee, J. S.; Jeong, E. D.; Hong, T. E.; Yoon, J. H.; Jin, J. S.; Kim, H. G. *Journal of the Korean Physical Society* **2007**, *51*, S22-S26.
9. Anandan, S.; Kathiravan, K.; Murugesan, V.; Ikuma, Y. *Catalysis Communications* **2009**, *10*, 1014.
10. Dunnill, C. W.; Parkin, I. P. *Dalton Transactions* **2011**, *40*, 1635.
11. Park, Y.; Kim, W.; Park, H.; Tachikawa, T.; Majima, T.; Choi, W. *Applied Catalysis B: Environmental* **2009**, *91*, 355.
12. Loganathan, K.; Bommusamy, P.; Muthaiahpillai, P.; Velayutham, M. *Environmental Engineering Research* **2011**, *16*, 81-90.
13. Bayati, M. R.; Aminzare, M.; Molaei, R.; Sadrnezhaad, S. K. *Materials Letters* **2011**, *65*, 840.
14. Nah, Y.-C.; Paramasivam, I.; Schmuki, P. *ChemPhysChem* **2010**, *11*, 2698.
15. Janotti, A.; Varley, J. B.; Rinke, P.; Umezawa, N.; Kresse, G.; Van De Walle, C. G. *Physical Review B - Condensed Matter and Materials Physics* **2010**, *81*.
16. Batzill, M.; Katsiev, K.; Gaspar, D. J.; Diebold, U. *Physical Review B - Condensed Matter and Materials Physics* **2002**, *66*, 2354011-23540110.
17. Wang, G.; Wang, H.; Ling, Y.; Tang, Y.; Yang, X.; Fitzmorris, R. C.; Wang, C.; Zhang, J. Z.; Li, Y. *Nano Letters* **2011**, *11*, 3026.
18. Zheng, L. *Sensors and Actuators B: Chemical* **2003**, *88*, 115.
19. Ni, Z.; Jun Jun, C.; Shima, H.; Akinaga, H. *Electron Device Letters, IEEE* **2012**, *33*, 1009.
20. Zhou, W.; Zhong, X.; Wu, X.; Yuan, L.; Shu, Q.; Xia, Y. *Journal of the Korean Physical Society* **2006**, *49*, 2168-2175.
21. Koh, C.-W.; Lee, U. H.; Song, J.-K.; Lee, H.-R.; Kim, M.-H.; Suh, M.; Kwon, Y.-U. *Chemistry - An Asian Journal* **2008**, *3*, 862.
22. Grosso, D.; Soler-Illia, G. J. d. A. A.; Crepaldi, E. L.; Cagnol, F.; Sinturel, C.; Bourgeois, A.; Brunet-Bruneau, A.; Amenitsch, H.; Albouy, P. A. Sanchez, C. *Chemistry of Materials* **2003**, *15*, 4562.
23. Lee, U. H.; Kim, M. H.; Kwon, Y. U. *Bulletin of the Korean Chemical Society* **2006**, *27*, 808-816.
24. Wu, C.-W.; Ohsuna, T.; Kuwabara, M.; Kuroda, K. *Journal of the American Chemical Society* **2006**, *128*, 4544.
25. Šćepanović, M.; Grujić-Brojčin, M.; Miriæ, M.; Dohčević-Mitrović, Z.; Popović, Z. V. *Acta Physica Polonica A* **2009**, *116*, 603-606.
26. Lei, Y.; Liu, H.; Xiao, W. *Modelling and Simulation in Materials Science and Engineering* **2010**, 18.
27. Khan, S. U. M.; Al-Shahry, M.; Ingler, W. B. *Science* **2002**, *297*, 2243-2245.
28. Chen, Z.; Jaramillo, T. F.; Deutsch, T. G.; Kleiman-Shwarsctein, A.; Forman, A. J.; Gaillard, N.; Garland, R.; Takanabe, K.; Heske, C.; Sunkara, M.; McFarland, E. W.; Domen, K.; Miller, E. L.; Turner, J. A.; Dinh, H. N. *Journal of Materials Research* **2010**, *25*, 3.
29. Eppler, A. M.; Ballard, I. M.; Nelson, *J. Physica. E* **2002**, *14*, 197.
30. Chester, P. F.; Bradhurst, D. H. *Nature* **1963**, *199*, 1056.
31. Breckenridge, R. G.; Hosler, W. R. *Phys. Rev.* **1953**, *91*, 793.
32. Varghese, O. K.; Grimes, C. A. *Solar Energy Materials and Solar Cells* **2008**, *92*, 374.
33. Hartmann, P.; Lee, D.-K.; Smarsly, B. M.; Janek, J. *ACS Nano.* **2010**, *4*, 3147.
34. Smarsly, B.; Grosso, D.; Brezesinski, T.; Pinna, N.; Boissière, C.; Antonietti, M.; Sanchez, C. *Chemistry of Materials* **2004**, *16*, 2948.
35. Ko, Y.-S.; Koh, C.-W.; Lee, U. H.; Kwon, Y.-U. *Microporous and Mesoporous Materials* **2011**, *145*, 141.
36. Wu, Q. L.; Rankin, S. E. *Journal of Sol-Gel Science and Technology* **2011**, *60*, 81-90.